CODE-TO-CODE COMPARISONS FOR THE BLIND-TEST ACTIVITY OF THE TILTAERO PROJECT

Antonio Visingardi
CIRA
Capua - Italy

Julien Decours
ONERA
Chatillon - France

Walid Khier
DLR
Braunschweig - Germany

Spyros Voutsinas
NTUA
Athens - Greece

Abstract

The present paper illustrates the results obtained so far by CIRA, DLR, NTUA and ONERA during a blind-test activity performed in the framework of WP1 of the European research project TILTAERO (TILTrotor interactional AEROdynamics). The aim of the work package is to evaluate the capabilities of the prediction tools applied for the analysis of the interactional aerodynamics of a tilt rotor configuration. Two BEM methodologies, differing with respect to the wake modelling, an unsteady RANS and a quasi-steady RANS CFD methodologies have been applied by the authors for this purpose. The paper provides a synthetic description of the TILTAERO project and illustrates the main aspects of the blind-test activity. The main features of the numerical methodologies applied are also described. The analysis is performed by illustrating the numerical results obtained for three different test conditions of the TILTAERO wind tunnel mock-up in terms of quasi-steady, time-averaged and unsteady pressure distributions as well as quasi-steady, time-averaged and unsteady normal forces acting on the configuration. These results, obtained prior to the production and release of the relevant experimental data base, have provided useful indications of the complex interactional phenomenology.

List of Symbols

c	Airfoil chord
CD	Drag coefficient
CL	Lift coefficient
CN	Normal force coefficient
CNavg	Time-averaged Normal force coeff.
Cp	Pressure Coefficient
Cpavg	Time-averaged Pressure coefficient
Cpu	Unsteady component of Pressure coeff.
CT	Prop rotor thrust coefficient
L	Wing span length
Psi	Azimuthal station
r	Local blade radius
R	Blade radius
y	Local wing span station
φ	Velocity potential

Introduction

The tilt rotor is an aircraft which combines the advantages of vertical takeoff and landing capabilities, specific to the helicopters, with the forward speed and range of a turboprop airplane. Such characteristics make this aircraft able to provide high-speed, long-range flight, coupled with runway independent operations thus having a significant potential to considerably reduce airport congestion problems. By virtue of these attractive peculiarities, the European Union funded a series of research projects, which could investigate the various technological aspects dealing with the tilt rotor aircraft, with the specific aim to increase the competitiveness of the European helicopter industry.

The TILTAERO project

In this framework, the four-year research project TILTAERO (TILTrotor interactional AEROdynamics), funded by the European Union under the "Competitive and Sustainable Growth" Programme, Contract Nr. G4RD-CT-2001-00477, Ref 1, aims at the development of a common European database capable to cover the main aerodynamic interactional phenomena arising during the different flight conditions of a tilt rotor aircraft. This database is employed to validate the prediction tools in order to assess their capabilities in capturing the interactional phenomena and to address the research activity to those areas revealing lack of knowledge.

The research objectives addressed by the TILTAERO project will provide:

- a range of high performance and validated analytical tools that will enable designers to accurately predict the aerodynamic efficiency of the tilt rotor wing surfaces (fixed and rotating);
- a detailed investigation of the aerodynamic interactional phenomena in different tilt rotor flight conditions, providing high quality wind tunnel test data to increase the designer's knowledge about aircraft efficiency in this field.

The consortium includes the four European

helicopter manufacturers: Agusta S.p.A. (Italy), co-ordinator of the project; Westland Helicopters Ltd (UK); Eurocopter (France) and Eurocopter Deutschland (Germany); the IAI, Israel's aircraft manufacturer; four aerospace research centres: CIRA (Italy); DLR (Germany); NLR (The Netherlands) and ONERA (France), and the National Technical University of Athens, NTUA (Greece).

The project is organised in five work packages: WP1 - Aerodynamics Prediction Codes; WP2 - Powered full-span mock-up feasibility studies; WP3 - Powered half-span mock-up; WP4 - Wind Tunnel tests of the powered half-span mock-up; WP5 - Wind Tunnel tests analysis.

Objectives of the paper

The aim of this paper is to illustrate the results obtained so far during the TILTAERO blind-test activity by CIRA, DLR, NTUA and ONERA which have applied different methodologies for their investigations. For this purpose, the blind-test activity and the wind tunnel model are first described. The numerical methodologies applied by the authors are then illustrated and finally the results of the numerical investigations are shown and discussed.

The Blind-Test Activity

The theoretical-numerical TILTAERO activity is performed in the framework of WP1: "*Aerodynamics Prediction Codes*".

A large variety of prediction tools is available among the participating partners: from Flight Mechanics codes and panel methods, to the more sophisticated CFD Euler and Navier-Stokes computer codes. These existing tools, basically conceived for the aerodynamic analysis of the helicopters, were first critically assessed. A pre-test activity was then performed by some partners with the aim to assess the ability of their tools to model the interactional phenomenology of a tilt rotor-like configuration. For this purpose, the numerical-experimental comparisons were performed by exploiting the PROPWING database, Ref 2, and some results were reported in a paper presented at the 29th ERF in 2003, Ref 3. In parallel, a code adaptation activity was also performed in order to allow the tools to better model the interactional aerodynamics of a tilt rotor.

In this framework, the blind-test activity represents the last step of the numerical activity before starting the final validation of the prediction codes. The aim of this activity is then to make numerical investigations on the TILTAERO wind tunnel model prior to the production and release of the relative experimental data base. A set of seven blind-test cases has been chosen which range from hover to cruise including the conversion flight, Ref 4. The relative trim conditions were pre-calculated by Agusta by using an in-house code for aeroelastic predictions. For the fulfilment of this activity each partner was assigned a number of these blind-tests to analyze. The results of preliminary computations were presented at the IV ECCOMAS congress in 2004, Ref 5.

The Wind Tunnel Mock-up

The TILTAERO wind tunnel mock-up is a half-span 40% Mach-scaled model based on the advanced European tilt rotor concept. It is constituted by three main components: the four-bladed gimballed prop-rotor which has a diameter of 2.96 m; the tiltable nacelle; the wing which has a tapered plan form with flaps and a span length of 2.22 m. In order to reduce the prop-rotor download effects the wing is split into two parts: the inner wing which is fixed with respect to a fairing representing the fuselage and the outer wing which is able to independently tilt with respect to the fixed wing and the nacelle (Fig 1).

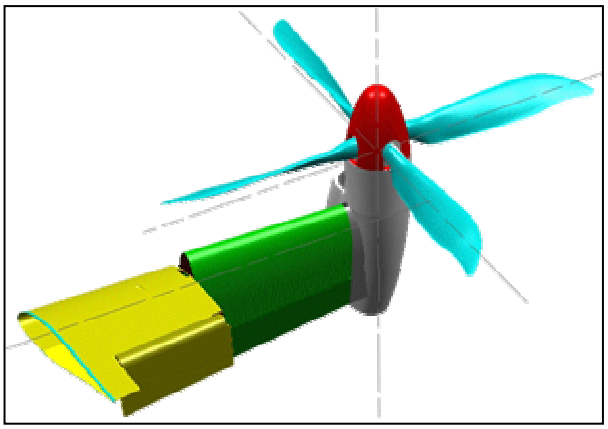

Fig 1: The TILTAERO half-span mock-up

The mock-up will be vertically mounted in the ¾-open test section of the DNW-LLF wind tunnel. The test campaign will cover a wide range of points of the flight envelope, from low speed helicopter mode to high speed airplane mode, with the parametric variation of component settings like the wing incidence and the tilt angle, the nacelle attitude, the rotor operating point. In order to allow the phenomena investigation the model will be fully instrumented. A number of unsteady pressure sensors will be located along five blade sections:

r/R=0.500; 0.750; 0.860; 0.940 and 0.970. Similarly, unsteady pressure sensors will be located along three wing sections: one on the fixed wing at y/L=0.508, towards the tip; one on the movable wing at y/L=0.672, towards the root, and the last at y/L=0.792, in the middle of the movable wing. Five additional unsteady pressure sensors will be spanwise located at the leading edge of the movable wing. Furthermore, the integrated loads on the prop rotor and wings will be measured through balances whereas blade moments and deformations will be derived from strain gauges measurements. Finally, steady pressure measurements on the wings and flow field measurements, made at selected conditions using the PIV technique, will complete the data base.

Description of the Methodologies

Two different methodologies have been applied by the authors: CIRA and NTUA have applied the Boundary Element Methodology (BEM) – differing with respect to the wake modelling - which assumes that the flow is incompressible and inviscid; DLR and ONERA have applied two flow solvers based on the more sophisticated Reynolds Averaged Navier-Stokes equations (RANS); DLR has performed unsteady computations whereas ONERA has used a quasi-steady approach where the prop-rotor is modelled by an actuator disc. A description of these methodologies is illustrated in the following.

CIRA - RAMSYS

The in-house developed CIRA computer code RAMSYS (Rotorcraft Aerodynamic Modelling SYStem), Ref 6, is an unsteady panel code for multi-body configurations based on Morino's boundary integral formulation.

The formulation consists in the solution of Laplace's equation, written in terms of the velocity potential φ with the classical boundary conditions according to which $\varphi = 0$ at infinity; the impermeability condition is satisfied on the body surface; the wake is not penetrated by the fluid and there is no pressure jump across its surface; the velocity potential jump $\Delta\varphi$ remains constant following a wake point x_w, and equal to the value it had when x_w left the trailing edge.

The value of $\Delta\varphi$ at the trailing edge is obtained by applying the Kutta-Joukowski hypothesis that no vortex filament exists at the trailing edge. For highly 3D and/or unsteady flows a correction of the classical Kutta condition, Ref 7, is applied in order to explicitly impose a zero pressure jump at the trailing edge.

The application of Green's function method to Laplace's equation yields a boundary-integral-representation for the velocity potential φ which models the body through a distribution of sources and doublets and the wake through a distribution of doublets only.

The helicopter geometry and the wake are respectively discretised by hyperboloidal quadrilateral panels, on which the unknown velocity potential, the normal-wash and the velocity potential jump are constant (zeroth-order formulation). By using the collocation method and setting the collocation points at the centroids of each element on the body geometry, the integral equation is replaced by an algebraic linear system of equations for the velocity potential φ which is finally solved by the application of a Conjugate Gradient Method (GMRES solver).

Compressibility is taken into account in the code by the application of the classical Prandtl-Glauert correction formula.

A time-marching free-wake model is implemented in RAMSYS and different vortex-core models are available to numerically stabilize the wake.

An interactional technique is implemented in RAMSYS in order to avoid the rising of unphysical solutions during the interactional process due to which the wake penetrates the body surface. The method, proposed by Clark and Maskew, Ref 8, consists in the cancellation of the doublet intensities $\Delta\varphi$ of those wake panels which penetrate the body or that are too close to the body so that they could induce excessive velocities in the near body panels.

The application of the pure free-wake model can determine an excessively chaotic vortical system which alters considerably the solution on the body. For this reason, in order to regularize the wake shape a simple progressive stiffening technique and a smoothing technique have been applied.

DLR – FlOWer

The computer code FLOWer solves the time dependent Reynolds (Favre)-Averaged Navier-Stokes equations in three dimensions using a finite volume, multi-block-based approach, Ref 9. The solution process is based on Jameson's method where a second order central scheme is used for the discretisation of the convective fluxes. A stabilizing blend of second and fourth order dissipation is added to the fluxes of the main flow equations. Alternatively, upwind AUSM/Van Leer scheme can be used to

discretise the convective fluxes as explained in Ref 10. Viscous fluxes are evaluated numerically by a second order central difference approximation.

A second order accurate dual time stepping approach is used to integrate the equations in time, Ref 11. Each physical time step, a steady flow problem is solved by advancing the discretised equations in a fictitious time using a multi-stage Runge-Kutta method. The solution process makes use of acceleration techniques like local time stepping, multigrid and implicit residual smoothing.

Turbulence effects may be accounted for in FLOWer by one of several statistical turbulence models, ranging from algebraic models to seven-equation differential stress models (RSM). The results presented in this paper were obtained by using a modified version of Wilcox's k-ω model, Ref 12.

The motion of the rotor blades relative to the rest of the configuration is accomplished by a moving overlapping Chimera technique, Refs 13-16.

Chimera implementation in FLOWer allows complex motion to be specified. Theoretically, an unlimited number (up to the code dimension limits) of hierarchies of relative motions can be specified in time, and applied to the different elements of the geometry. Each level of the hierarchy defines a separate reference frame in which motions can be specified independently of the inertial frame of reference, thus allowing any combination of translatory and rotary motions to be realized by a series of simple co-ordinate transformations.

To compute rotary wing flows efficiently, a low speed preconditioning was implemented in FLOWer following the idea presented in Ref 17.

NTUA – GenUVP

GenUVP is a time marching prediction code for flows around multi-body aircraft configurations, Refs 18-20. The modelling is based on an appropriate interpretation of the Helmholtz decomposition theorem. The potential part corresponds to the flow generated by the presence of moving solid boundaries while the rotational part corresponds to the flow induced by the wake. At the approximate level, the potential part is modelled by means of a source-dipole indirect integral representation based on the boundary element method. At every time step vorticity is released from the extremities of the solid boundaries in the free flow. Vorticity emission is carried out along prescribed lines which include the trailing edge of all the main lifting parts of the configuration and possibly part of their tip and/or root sections. The intensity of the vorticity which is released is determined by imposing a zero pressure jump across the emission lines. At the end of every time step the vorticity emitted during the last step is transformed into freely moving vortex blobs which evolve according to the vorticity transport equations written in material co-ordinates. GenUVP offers the possibility to also include the flexibility of the configuration, Ref 21. This is particularly important in helicopter and tilt rotor applications. In this connection fully non-linear coupling is performed so that the aerodynamic part provides the external loading to the structure while the structure feeds back the deformed geometry and the deformation velocities. In this case an iterative process during each time step is used in order to converge the complete system. Post processing add-on options to the baseline version of GenUVP include compressibility and boundary layer corrections, Refs 18, 22. They are both added by performing local calculations in a section-by-section basis. Input to this is the flow velocity over the section which is recorded in time.

ONERA - *elsA*

The ONERA object-oriented computational code *elsA* (Ensemble Logiciel de Simulation en Aérodynamique), Ref 23, solves the Reynolds averaged Navier-Stokes equations in a finite volume formulation on multiblock structured meshes. The solver is used for a large variety of configurations (aircraft, turbomachinery, helicopter, tiltrotor…).

The numerical parameters used to calculate the rotor/wing aerodynamic interaction are based on a 2^{nd} order Jameson scheme in space discretisation with a scalar artificial viscosity including Martinelli's correction combined with a LU-SSOR scalar relaxation implicit phase with backward Euler time integration. Among the several turbulence models available in *elsA*, the Wilcox k-ω model with SST correction has been used. The computations are initialised with 20 laminar iterations.

The simulation of a rotating machine (rotor, propeller…) can be simplified by modelling the rotor with a lifting surface, called "actuator disk", Ref 24. It represents the loads of the rotor which are averaged in time and applied on a surface grid in a steady flow computation. The actuator disk model is introduced into the code as a particular boundary condition where discontinuous aerodynamic quantities are prescribed. Due to the steady-state assumption, a great reduction of computational cost is achieved by

comparison with an unsteady computation of the flow around rotating blades. The boundary condition formulation behaves like a usual interface and the actuator disk source terms are simply added to residuals for the cells lying below the actuator disk surface. The source terms which model the discontinuities of the flow field are calculated by blade elements theories with the *HOST* software allowing either a uniform global lift or variations in the radial and azimuth directions on the disk (non-uniform actuator disk).

The construction of a structured multiblock mesh around complex geometries is difficult and needs a good know-how. The Chimera technique allows simplifying the process of mesh generation by using a background grid, the nacelle in this study, on which additional body parts, the two wings, the wind tunnel support and the actuator disk can be overlapped. The method consists in introducing classical overlapping boundary conditions and also masks conditions on body's areas which will influence the overlapped grids, Ref 25. Concerning the nacelle, a mask on the two wings, the wind tunnel support and the actuator disk boundary is applied. Then, the associated domains are masked and the data exchange are realised by interpolation in the vicinity of the mask. Among the several methods and parameters available to adapt the mask and interpolation to the configuration, we used the ADT method (Alternating Digital Tree) with one point outside the mask, made of cartesian elements.

Results and Discussion

Three test cases, selected from those planned for the TILTAERO blind-test activity, have been simulated by the authors: ID3 and ID4, concerning two different conversion flight conditions, and ID7 corresponding to a cruise flight. In particular, ID3 has been examined by DLR and ONERA whereas ID4 has been examined by CIRA and NTUA. Finally, ID7 has been examined by all the four authors. The description of these test cases and the analysis of the results obtained is presented in the following.

Trim Procedures

Different trim procedures have bee followed by the authors. DLR has fully relied on the Agusta pre-calculated control angles. CIRA and NTUA have modified the collective pitch only in order to get the time-averaged value of the thrust coefficient equal to the pre-calculated one. Finally, ONERA has imposed the pre-calculated forces and has derived their own control angles by the use of the HOST computer code.

Test Case ID3

Model set-up: The test case chosen by DLR and ONERA refers to a conversion flight with a nacelle tilt angle equal to 75.00^0. The fixed wing angle of attack is set at 3.00º and the movable wing is set at 10.29º. The prop rotor angular velocity is equal to 1382.5 RPM and the free stream velocity is 54.02 m/s. The nominal pre-calculated blade collective pitch is set at 11.330°.

Numerical discretisations: In ONERA computations the nacelle mesh is used as a background grid. The nacelle grid contains a total of about 3 million points distributed in 22 blocks with a first cell size of 3 microns. The fixed wing is meshed in a 'C-H' topology and has a total of about 1.4 million points distributed in 8 blocks whereas the tiltable wing has a total of about 1.3 million points distributed in 8 blocks. The wind tunnel support is meshed in a 'C-H' topology and has a total of about 500.000 points distributed in 10 blocks. The gaps between the wind tunnel support, the two half wings and the nacelle are also modelled. The actuator disk grid has a total of 150000 points distributed in 4 blocks. Computations were performed with no actuator disk, uniform actuator disk and non uniform actuator disk.

For DLR computations the configuration has been subdivided into 7 components: nacelle, movable wing, fixed wing + fairing, and the four blades. Multi-block structured grids have been generated around each component. The locally refined Cartesian background grid consists of 1.8 Million points and 409 blocks. The component grids had a total number of 6.6 Million points, and 54 blocks.

Analysis of the results: Fig 2 presents the convergence of the load coefficients evaluated by ONERA. On the fixed part of the wing (solid lines) the lift increases with both actuators (about 8%). On the movable wing (dashed lines) the uniform actuator decreases the lift coefficient by about 20% because of a large stalled region, whereas the non uniform actuator induces only a 6% decrease because of a more concentrated downwash. The oscillations of the load coefficients are due to complex airflow instabilities.

Fig 3 presents the pressure coefficient and the skin friction lines on the wings for the no, uniform and non uniform actuator disk cases. A large separation region can be observed on the upper side of the movable wing which creates an important loss of lift. This behaviour is also confirmed in DLR results in terms of streamlines. Indeed, Fig 4 shows computed streamlines patterns on the upper and lower surfaces

of the wing, respectively. Three dimensional effects are evident on both wing parts close to the inner and outer ends. On the upper surface of the moveable wing part, traces of two separation zones can be identified. The nacelle blocks the flow from rolling up over the wing tip, except for the rear outer corner. The second separation zone starts at the articulation axis on the outer upper edge of the moveable wing, and moves downstream as the inner edge is approached

Fig 5 presents ONERA 3D visualisations of the stalled region on the movable wing which seems to be generated by the geometry of the wing-nacelle junction plus a high wing angle of attack.

Similarly, the surface streamlines computed by DLR in this zone indicate massive flow separation from the nacelle, as can be seen in Fig 6. The separation region extends over the whole wing span, and merges with inner tip vortex. The latter is generated as a result of tilting the wing, and leakage of the flow through the gap between the wing parts. The rotor, which is not illustrated in the figures, has very little influence on the flow structure over the wing, as indicated by Fig 7. The figure shows a cross section of the wake at x=0.6 D (where D is the rotor diameter) and azimuth angle equal to 96^{o}. From the figure it can be clearly seen that the rotor wake is rapidly convected downstream away from the wing, and no interaction between the rotor and wing and/or nacelle wakes can be observed.

The normal force repartition along the wing span evaluated by ONERA and DLR, Figs 8 and 9, confirm the important loss of lift.

Fig 10 illustrates a comparison of the time-averaged pressure distributions evaluated by ONERA and DLR. A very similar pressure distribution can be seen on the fixed wing, section 1 (y/L=0.508). The observed small differences in values are probably due to using different grids, turbulence models and codes. Significant differences between the time accurate (DLR) and actuator disc results (ONERA) can instead be noticed for the two stations on the movable wing. The same pressure pattern observed at y/L=0.508 can be found in the time accurate case, in line with the previously mentioned negligible interaction between the wake of the prop rotor and the separated flow zone on the wing. ONERA results reveal steeper adverse pressure gradients downstream of the suction peak, and clear pressure fluctuations downstream x/c=0.4. Furthermore, the DLR unsteady pressure coefficients illustrated in Fig 11 supports this claim and show very weak unsteady behaviour for the time accurate computations.

The different rotor controls used for FLOWer and *elsA* codes can be a further explanation of these fundamental differences between the DLR and ONERA results.

Test Case ID4

Model set-up: The test case chosen by CIRA and NTUA refers to a conversion flight with a nacelle tilt angle equal to 59.95^{0}. The fixed wing angle of attack is set at 2.95º and the movable wing is set at 3.64º. The prop rotor angular velocity is equal to 1382.5 RPM and the free stream velocity is 72.02 m/s. The nominal pre-calculated blade collective pitch is set at 17.0^{0}

Numerical discretisation: CIRA computation has been performed with a body (wing+nacelle) discretisation equal to 3026 panels whereas each blade has been discretized by 40x16 panels. A free-wake modelling has been employed in order to evaluate the interactional process between the wake system and the body components. Three wake spirals have been modelled with an azimuth discretisation fixed at 5^{0}. Six rotor revolutions have been performed in order to reach a fully periodic solution. NTUA has used a grid of 2827 panels on the body and a grid of 30x13 panels on each blade. Four rotor revolutions have been performed at the end of which a reasonable convergence has been achieved. A fifth revolution would be probably necessary for full convergence.

Analysis of the results: CIRA and NTUA computations have been performed by slightly reducing the collective pitch only respectively of 0.4% and 1.47%. Fig 12 illustrates that the periodicity of the solution has been reached after three revolutions. The 4/rev behaviour due to the four-bladed rotor configuration can also be easily detected. An over-estimation in NTUA results can be observed. This is due to the trimming procedure which in the case of NTUA was based on isolated rotor configurations.

Fig 13 illustrates the normal force coefficient time history evaluated on the prop rotor blade in presence of the wing+nacelle. Apart from the radial station at 50% of the span, where a large undershoot is obtained by NTUA, the results at the other radial stations indicate a good qualitative agreement between CIRA and NTUA predictions.

A comparison between CIRA and NTUA computations of the time-averaged normal force coefficient along the wing span is illustrated in Fig 14. The increase in the load toward the wing tip region,

more evident in CIRA results, weaker in NTUA results, is basically due to the influence of the nacelle which, with its high incidence (approx. 60°), accelerates the flow.

In order to better represent the unsteady pressure distributions on the wing, the time-averaged part has been separated from the purely unsteady one. The two parts have been then plotted separately for three reference wing sections: section 1 - y/L=0.508; section 2 - y/L=0.672; and section 3 - y/L=0.792. The analysis of the time-averaged pressure coefficients at the three reference wing sections (Fig 15) indicates for both CIRA and NTUA computations an increase of the expansion peak on the upper part of the wing moving toward the wing tip which can be justified by the strong influence that at this test condition is exerted by the nacelle.

The unsteady pressure coefficient time history at the three reference wing sections is represented in Fig 16. In order to evaluate the wing regions that are more influenced by the wake-body interactional process three representative chord wise locations have been chosen: the first one located in the vicinity of the leading edge (x/c = 2.5%); the second located approximately at the quarter chord (x/c = 21.5%) and the third one located toward the wing section trailing edge (x/c = 63.5%). In general, it can be observed that section 1, located on the fixed wing, is only slightly influenced by the unsteadiness of the flow field. Conversely, passing to sections 2 and 3 the unsteadiness become more pronounced due to the direct influence of the prop rotor wake system. The first half of the wing section plays the most important role during the interaction with the wake whereas the pressure fluctuations tend to decrease toward the trailing edge. The upper part of the movable wing is more directly subjected to the wake impingement thus giving rise to higher pressure fluctuations than the lower part of the wing. The blade passages in front of the wing can be detected by the 4/rev periodicity of the pressure signals. Finally, comparing the two sets of results, a phase shift is seen while the amplitudes are more or less comparable with CIRA's results giving higher peaks at the leading edge of section 3. These differences are attributed to the way each code handles wake impingement on the wing. RAMSYS is based on a filament representation of wake while GenUVP is using vortex blobs. Regardless the type of approximation each code uses, when the wake vorticity approaches the wing surface, it will undergo intense stretching. In RAMSYS this is sensed on the length and orientation of the filaments while in GenUVP the effect will change the intensity and the direction of the vorticity carried by the vortex blobs. So in an approximate calculation the way vorticity is divided over the two sides of the wing will be different. Then, concerning the phase shift, this is related to the rotor slipstream which is different. The definition of the simulations was set so that each code gives the foreseen thrust. The result was a different collective pitch. As a result the convection of the rotor wake is different and also different the time and location the wake impinges the wing surface.

Test Case ID7

Model set-up: The test case performed by all the authors refers to a cruise flight with a nacelle tilt angle equal to 0.30^0. Both the fixed wing and the movable wing angles of attack are set at 3.30º. The prop rotor angular velocity is equal to 1382.5 RPM and the free stream velocity is 72.02 m/s. The nominal pre-calculated blade collective pitch is set at 24.467°.

Numerical discretization: CIRA computation has been performed with a body (wing+nacelle) discretization equal to 2934 panels. All the other parameters have been kept equal to the ID4 test case. Analogously, the ONERA mesh system has been kept equal to the ID3 test case .NTUA used a grid of 2803 panels on the body and a grid of 30x13 panels on each blade. Four rotor revolutions have been performed at the end of which a convergence has been achieved. The DLR meshing has been kept the same as ID3 test case with the only exception of the locally refined Cartesian background grid which now consists of 1.5 Million points and 363 blocks.

Analysis of the results: Fig 17 presents the ONERA convergence history of averaged residuals for the cruise computation. The residuals decrease by about four orders of magnitude and the convergence curve shapes are very satisfactory.

The convergence of the computations has been also confirmed through the load coefficients history. On the movable wing (Fig 18, dashed lines), the lift coefficient (C_L) is slightly increased by the actuator disk (+3%) and increased again with the non uniform actuator disk (+2.4%). The drag coefficient (C_D) is increased with the uniform actuator disk but decreases with the non uniform one. These evolutions (about 5%), with the non uniform actuator disk, are a result of the induced velocity generated by the rotor downwash. The same behaviour is found on the fixed wing for the drag (Fig 18, solid lines) but the loads variations are less pronounced because the wing is not located in the rotor downwash. However the loads variations between the three configurations

(no, uniform and non uniform actuator disk) are small because the rotor thrust is small in cruise flight condition.

The convergence histories of the BEM computations are instead expressed in terms of the thrust coefficient time histories as illustrated in Fig 19. In order to obtain the same average value of the nominal pre-calculated thrust coefficient, both CIRA and NTUA computations have been performed by reducing the collective pitch only (respectively 6.6% for CIRA and 1.63% for NTUA). CIRA computation reach the converged fully 4/rev periodicity after the first revolution whereas NTUA shows a converged solution since the start of the computation. Despite the average values are the same, NTUA results show higher amplitude.

Fig 20 illustrates the normal force coefficient time history evaluated by CIRA and NTUA on the prop rotor in presence of the wing+nacelle. It is evident the influence of the wing around 270°. Despite the similar behaviour between the two sets of predictions, there response on the blade during its passage in front of the wing is different: CIRA's results indicate only an increase in the load whereas in NTUA's results the increase in the loading is followed by a decrease.

Fig 21 presents the ONERA time-averaged normal force coefficient along the wing span on the tilt rotor wings. The uniform actuator disk has a large influence zone whereas the non uniform actuator disk downwash effect is more concentrated on the movable wing. It can also be observed that the influence of the gap on the pressure coefficient extends to about 10% chord on both sides of the gap.

A comparison of the time-averaged normal force coefficient along the wing span of the tilt rotor wings is illustrated in Fig 22. CIRA estimation of the load is lower but has a qualitative behaviour similar to the one evaluated by NTUA. ONERA and DLR results have approximately the same qualitative behaviour with only a slight quantitative difference in the loads which are higher in DLR results. ONERA and NTUA results agree fairly well on the movable part of the wing whereas differ on the fixed wing where a decrease in the NTUA loads can be observed such that it approaches the CIRA result in proximity of the wing root. This is likely due to the different treatment of the wing support. All simulations have added the end plates. ONERA has added the full support followed by a wallslip while CIRA and NTUA did not add the tunnel wall. The computations indicate that the end plates are small and they will not alleviate the effect of the tip vortex. Of course the presence of the tunnel wall which is very close will take over. In future computations it seems necessary for CIRA and NTUA to add the tunnel wall as symmetry plane.

The analysis of the time-averaged pressure coefficients at the three reference wing sections, Fig 23, confirms the under estimation in CIRA results. The Cp distribution on the lower part of the wing sections evaluated by CIRA and ONERA agree very closely. DLR and ONERA are in very satisfactory agreement.

The unsteady pressure coefficient time history at the three reference wing sections is represented in Fig 24. As expected, the unsteadiness of the flow is in this case very mild. Nevertheless, it can be however observed that sections 2 and 3 are more affected by the unsteadiness of the flow due to the direct influence of the prop rotor wake system. The first half of the wing section plays the most important role during the interaction with the wake whereas the pressure fluctuations tend to decrease toward the trailing edge. In CIRA results the upper part of the movable wing is more directly subjected to the wake impingement thus giving rise to a higher amplitude of the pressure signal than the lower part of the wing. The blade passages in front of the wing can be detected by the 4/rev periodicity of the pressure signals. The comparison between CIRA and NTUA computations indicate different qualitative predictions of the interactional process mainly at the leading edge region (x/c = 2.5%). DLR results indicate the presence of a significant unsteadiness of the flow only at the leading edge of sections 2 and 3 where the agreement with both CIRA and NTUA results is fair in terms of amplitude and phase for the upper side of the wing. A phase shift on the lower side is observed between DLR results and CIRA / NTUA results which can be due to the different modelling of the wake: explicit and potential in CIRA and NTUA methods; resulting from the RANS computation of the flow field in DLR analysis.

Conclusions

Numerical simulations using models of varying complexity have been presented for a 40% Mach-scaled partial tilt rotor configuration. Despite the complexity of the flow and the differences between the models, qualitative agreement has been obtained while the differences have been explained. Furthermore, valuable experience has been acquired in view of the final pre-test calculations as well as the validation against the forthcoming wind tunnel tests.

Summarizing, the following conclusions have been drawn from this exercise:

a) With the exception of the ID3 time accurate computation, the rotor slipstream generally affects mainly the movable wing;

b) the nacelle plays an important role in increasing the lift of the movable wing in agreement with the findings on the PROPWING configuration, Ref 3;

c) the size of a simple end plate is not sufficient to cancel the effect of the root vortex of the fixed wing. It has become clear that it is necessary to include the tunnel wall in order to get zero lift cross derivative at the root;

d) the correct evaluation of the slipstream of the rotor represents a major task for the specific models. RAMSYS and GenUVP have included compressibility effects by applying the Prandtl-Glauert's correction which is not appropriate at high Mach numbers. *elsA* uses an actuator model and therefore results are directly dependent on the aerodynamic data used in the look up tables. FLOWer computations by DLR would be of major significance due to the nature of the methodology but however they fully rely on the pre-calculated trim conditions unlike the other ones. All these differences indicate that it is not expected a detailed agreement in the unsteady characteristics of the flow in the different simulations. In particular, significant differences have been found between the time accurate and actuator disc computations for ID3. While the actuator disc results show significant impact of the rotor on the upper surface of the movable wing, the time accurate computations did not indicate any significant interaction between the rotor and nacelle/wing wakes. This is most probably a direct result of using different rotor trim conditions for the two approaches, leading to different rotor wake characteristics in both cases.

From a methodological point of view, the conclusion of the different computational models is to be regarded as an important step towards a better understanding of the flow mechanisms governing the behaviour of the tilt rotor aircraft concept. In particular the significant difference in run-time cost between the different codes allows on one hand the systematic analysis of this type of aircraft while on the other the fine resolution with much more expensive CFD models.

Acknowledgments

This work is partly supported by the European Union under the Competitive and Sustainable Growth Programme in the 5th Framework, Contract Nr. G4RD-CT-2001-00477 (TILTAERO project).

References

1. Agusta S.p.A., "Tilt Rotor Interactional Aerodynamics – TILTAERO – Project Nr. GRD1 2000-25610 : Annex I, Description of Work," December 2000;
2. Voutsinas, S.G., "The PROPWING Database," Doc. Nr. TILTAERO/WP1/NTUA/R-01/B, January 2002;
3. Visingardi, A., "TILT rotor AEROdynamics: A comparative study of a BEM methodology with the PROPWING database," 29th European Rotorcraft Forum, Friedrichshafen, D, September 2003;
4. Saporiti, A., "Trim conditions for blind tests," Doc. Nr. TILTAERO/WP1/AGUSTA/R-03/B, January 2002;
5. Visingardi, A., Khier, W., Decours J., "The Blind-test activity of TILTAERO project for the numerical aerodynamic investigation of a tilt rotor," IV Eccomas Congress, Jyväskylä, SU, July 2004;
6. Visingardi, A., D'Alascio, A., Pagano A., and Renzoni, P., "Validation of CIRA's Rotorcraft Aerodynamic Modelling SYStem with DNW Experimental Data," 22nd European Rotorcraft Forum, Brighton, UK, September 1996;
7. D'Alascio, A., Visingardi, A., and Renzoni, P., "Explicit Kutta Condition Correction for Rotary Wing Flows," 19th World Conference on the Boundary Element Method, Rome, Italy, September 1997;
8. Clark, D.R., and Maskew, B. "Calculation of Unsteady Rotor Blade Loads and Blade/Fuselage Interference," II International Conference on Rotorcraft Basic Research, College Park, U.S.A., February. 1988;
9. Kroll, N., Rossow, C.C., Becker, K., Thiele, F., "The MEGAFLOW project," Aerospace, Science and Technology, Vol4, pp. 223-237, 2000;
10. Radespiel, R., Kroll, N., "Accurate Flux Vector Splittings for Shocks and Shear Layers," Journal of Computational Physics, 121, pp. 66-78, 1995;
11. Heinrich, R., Pahlke, K., Bleecke, H., "A Three-Dimensional Dual-Time Stepping Method for the Solution of the Unsteady Navier-Stokes Equations," Proceedings of the Conference on Unsteady Aerodynamics, July 17-18th, 1996,

London, UK;
12. Wilcox, D.C., “Reassessment of the Scale-Determining Equation for Advanced Turbulence Models,“ AIAA Journal, vol. 26, no. 11;
13. Schwarz, T., “Berechnung der Umströmung einer Hubschrauber-Rumpf-Konfiguration auf der Basis der Euler-Gleichungen mit der Chimären-Technik,“ DLR Internal Report IB-NR 129-97/23;
14. Meakin, R.L., “Moving Body Overset Grid Methods for Complete Aircraft Tiltrotor Simulations,” AIAA Paper 93-3350;
15. Stangl, R., “Ein Eulerverfahren zur Berechnung der Strömung um einen Hubschrauber im Vorwärtsflug,“ Dissertation, Universität Stuttgart, Institut für Aerodynamik und Gasdynamik, 1996;
16. Khier, W., Le Chuiton, F., Schwarz, T., “Navier-Stokes Analysis of the Helicopter Rotor-Fuselage Interference in Forward Flight,” CEAS Aerospace Aerodynamics Research Conference, June 2002, Cambridge, UK;
17. Turkel, E., Radespiel, R., Kroll, N. “Assessment of Preconditioning Methods for Multidimensional Aerodynamics,” Computers and Fluids, Vol.26, No. 6, pp. 613-634, 1997;
18. Voutsinas, S.G., Triantos, D.G. “High resolution aerodynamic analysis of full helicopter configurations”,25th ERF, Rome, paper C-11, 1999
19. Huberson, S., Voutsinas, S.G. “Particles and grid” Computers and Fluids, 31, 607-625, 2002
20. Voutsinas, S.G. “Vortex Methods in Aeronautics: How to make things work”, Proc. CFD-2004 Conference, Ottawa, Canada, 2004
21. Dieterich, O., Langer, H-J, Schneider O.,Imbert, G. Hounjet, M., Riziotis, V., Cafarelli, I.,Calvo R., Clerc, C., Pengel, K. “HeliNoVI: Current Vibration Research Activities”, 31st ERF, Florence, Italy, 2005
22. Voutsinas S. G., Riziotis V. A. “A Viscous-Inviscid Interaction Model for Dynamic Stall Simulations on Airfoils”, 37th Aerospace Sciences Meeting and Exhibit, Reno, January 11-14, 1999, AIAA paper 99-0038;
23. Cambier, L., Gazaix, M., “*elsA*: An efficient object-oriented solution to CFD complexity,” 40th AIAA Aerospace Science and Exhibit, Reno, NV, USA, 2002;
24. Renaud, T., “CHANCE project: Application of the actuator disk model for rotor/fuselage interaction computations with the *elsA* software,”Technical Report ONERA RT64/06082, April 2003;
25. Benoît, C., Le Pape, M.-C., Jeanfaivre, G., “Improvement of the robustness of the Chimera method,” Exhibit, Saint-Louis, USA, June 2002;

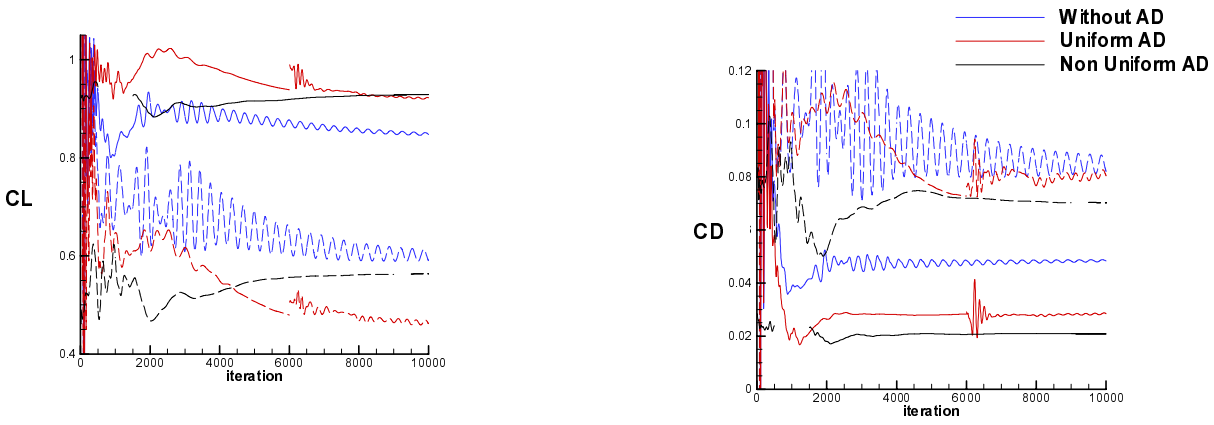

Fig 2: ONERA Convergence history of the lift and drag coefficients on the fixed and movable wings for conversion flight ID3.

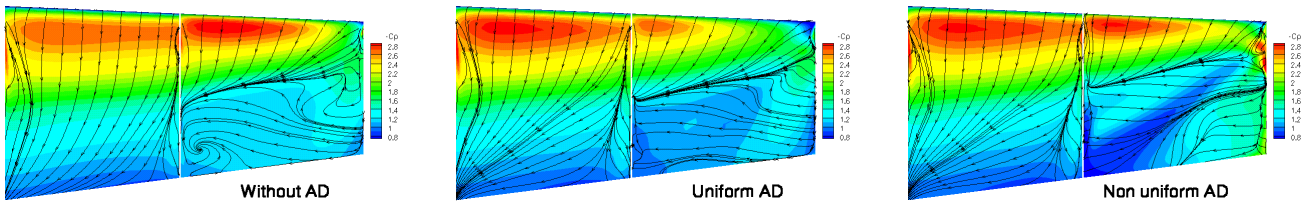

Fig 3: The ONERA three computations of the pressure coefficient and skin friction lines on the wings for conversion flight ID3

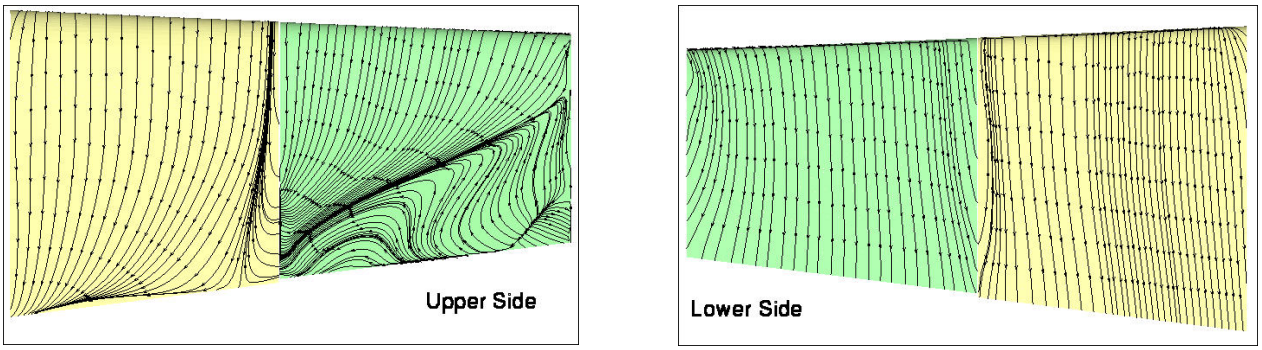

Fig 4: DLR computation of the streamlines on the wings for conversion flight ID3

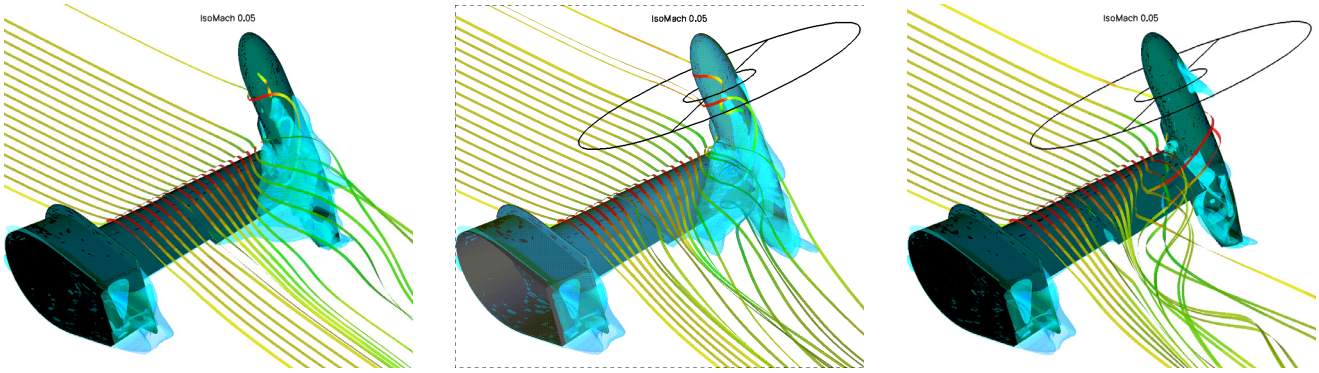

Fig 5: ONERA 3D visualisation of the stalled region on the movable wing for no, uniform and non uniform actuator disk for conversion flight ID3

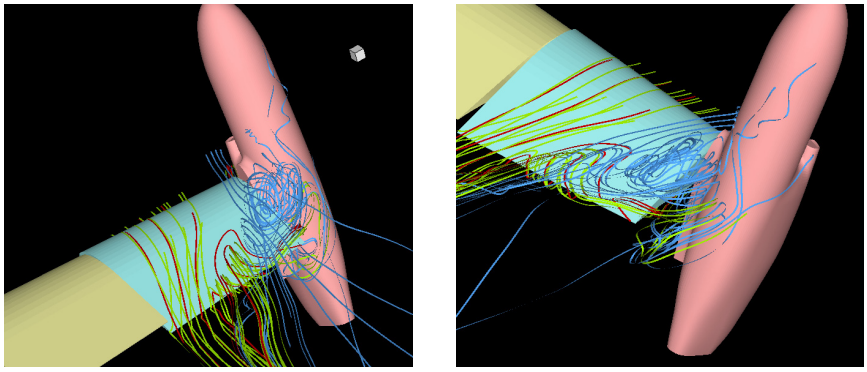

Fig 6: Flow structure over the wing surface for conversion flight ID3

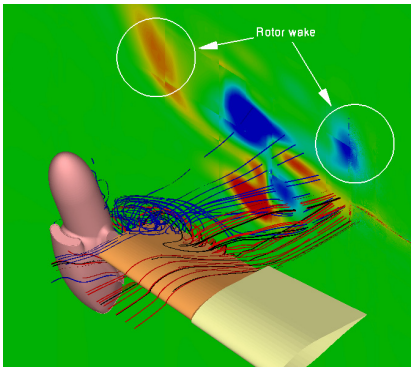

Fig 7: 3D streamlines and X-vorticity contours at x=0.6 D

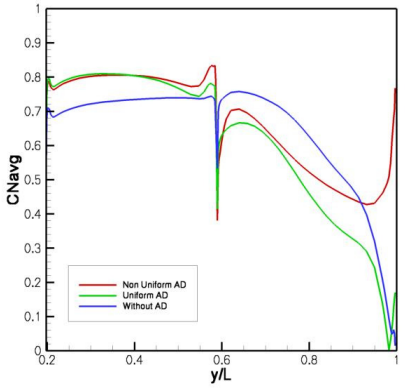

Fig 8: The ONERA three computations of the normal force coefficient along the wing span for conversion flight ID3

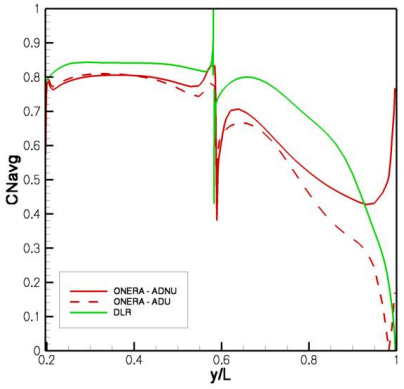

Fig 9: Comparison of the computed normal force coefficient along the wingspan for conversion flight ID3

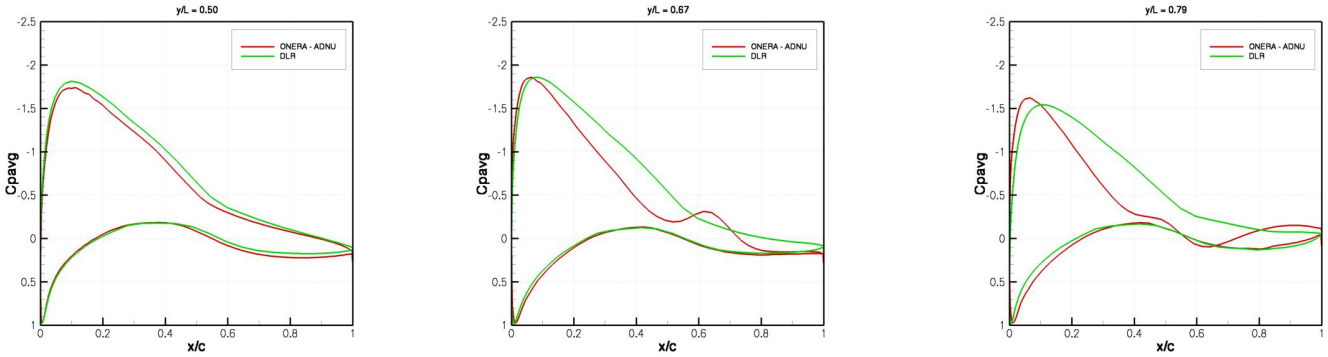

Fig 10: Comparison of the computed time-averaged pressure distributions on the wing for conversion flight ID3

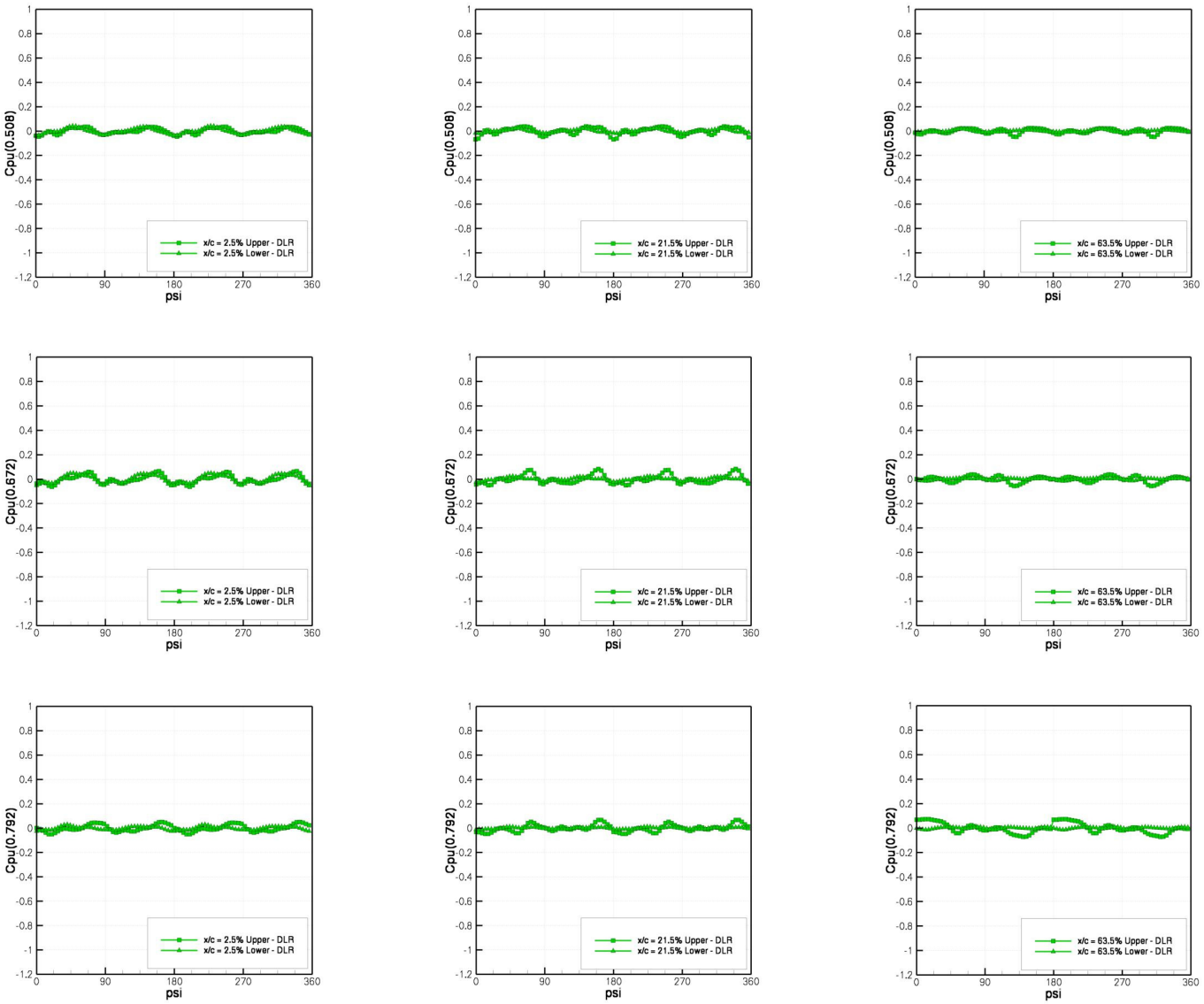

Fig 11: Comparison of the computed unsteady pressure coefficient time history on the wing for conversion flight ID3

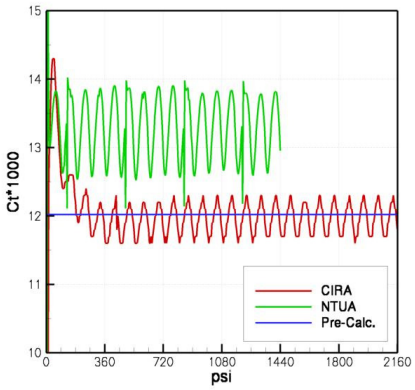

Fig 12: Comparison of the computed prop rotor thrust coefficient time history for conversion flight ID4

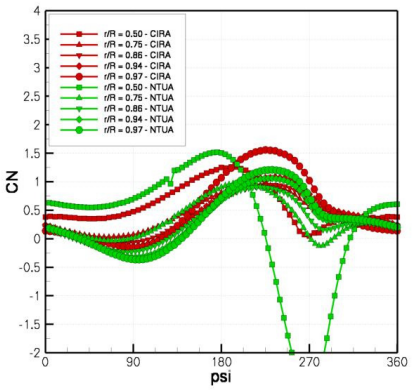

Fig 13: Comparison of the computed normal force coefficient time history on prop rotor blade for conversion flight ID4

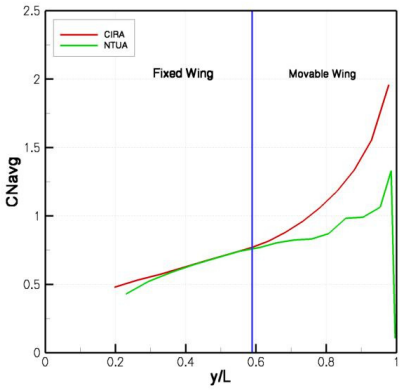

Fig 14: Comparison of the computed normal force coefficient along the wingspan for conversion flight ID4

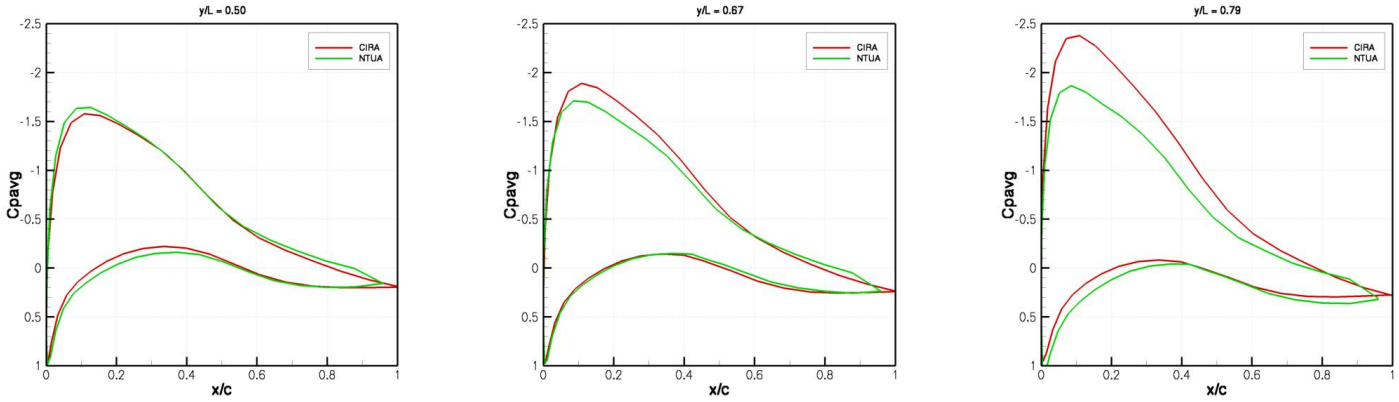

Fig 15: Comparison of the computed time-averaged pressure distributions on the wing for conversion flight ID4

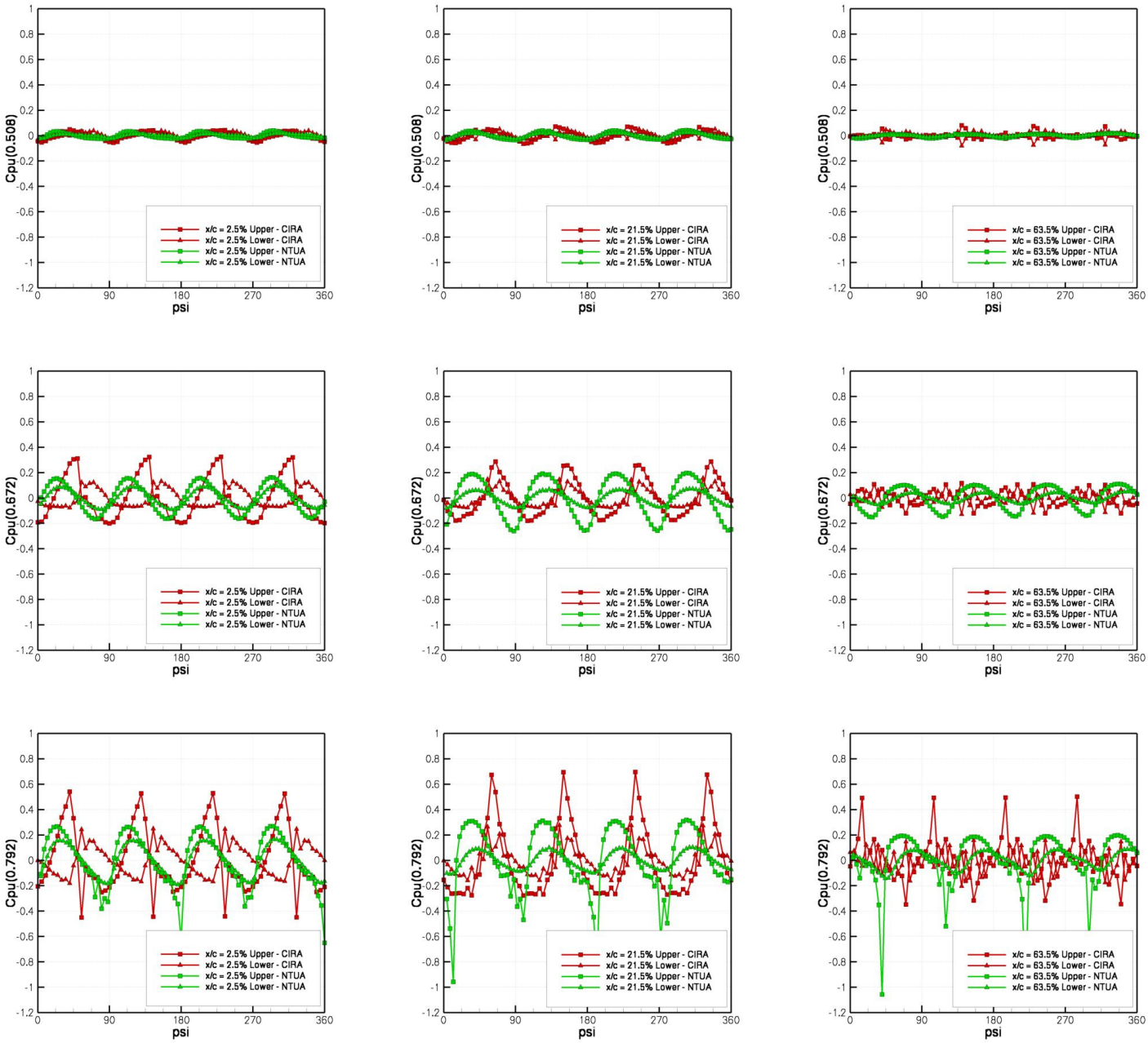

Fig 16: Comparison of the computed unsteady pressure coefficient time history on the wing for conversion flight ID4

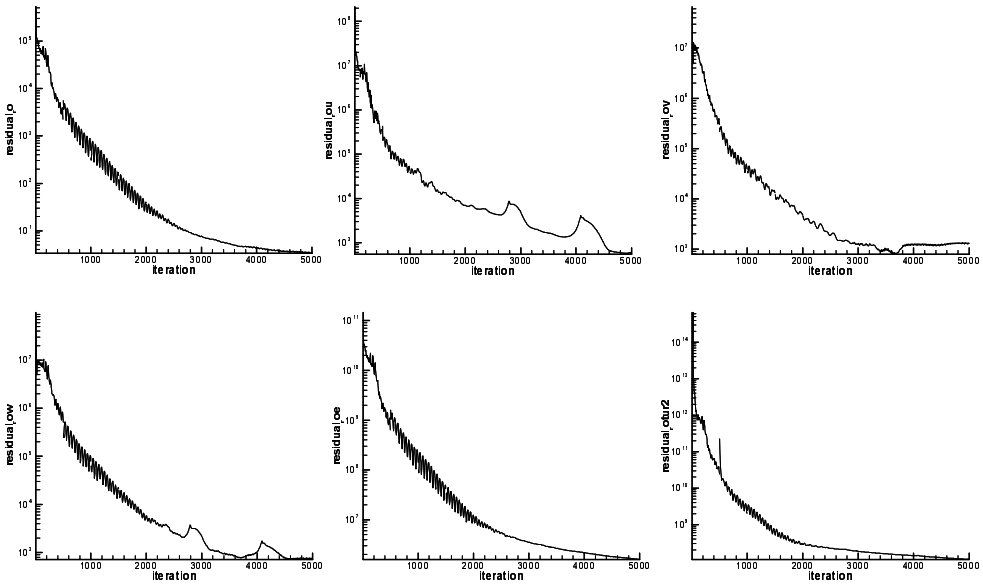

Fig 17: ONERA computations of the convergence history of the residuals for cruise flight ID7

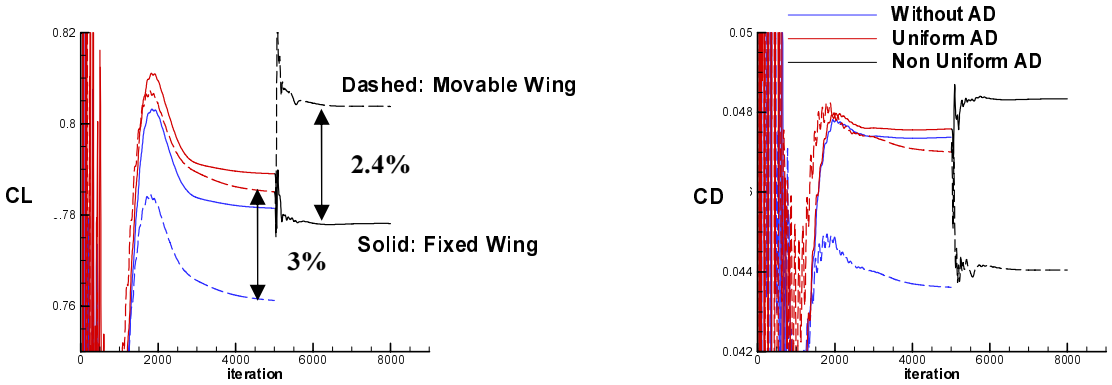

Fig 18: ONERA Convergence history of the lift and drag coefficients
on the fixed and movable wings for cruise flight ID7

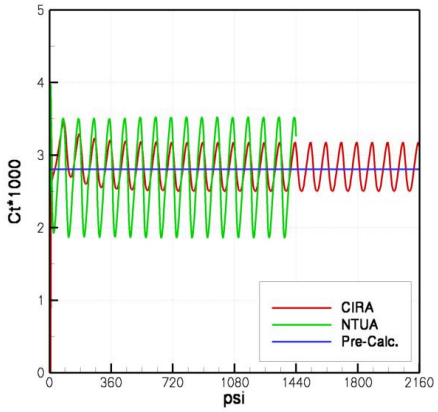

Fig 19: Comparison of the computed prop rotor thrust coefficient time history for cruise flight ID7

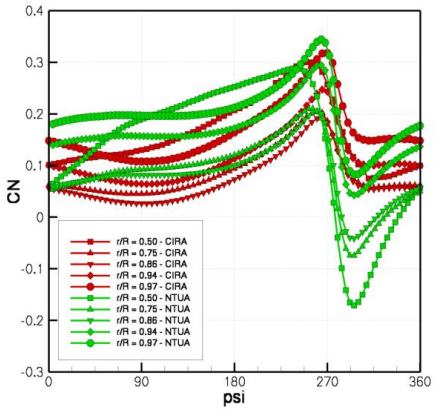

Fig 20: Comparison of the computed Normal force coefficient time history on prop rotor blade for cruise flight ID7

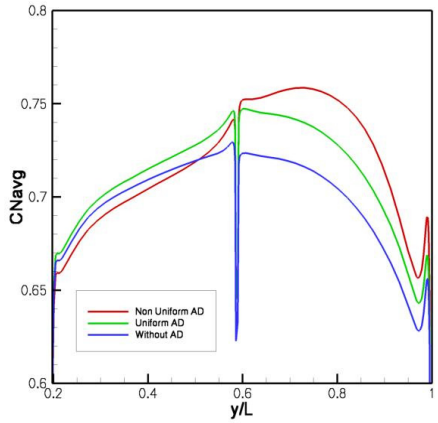

Fig 21: The ONERA three computations of the normal force coefficient along the wing span for cruise flight ID7

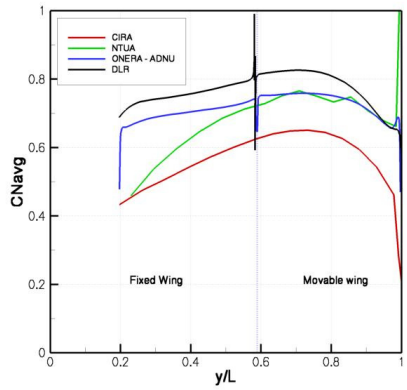

Fig 22: Comparison of the computed normal force coefficient along the wingspan for cruise flight ID7

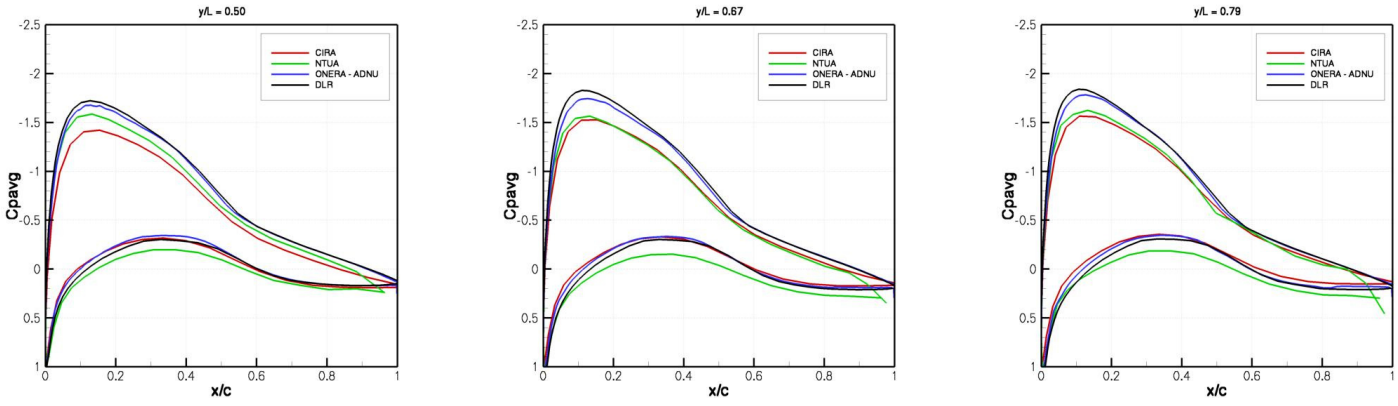

Fig 23: Comparison of the computed time-averaged pressure distributions on the wing for cruise flight ID7

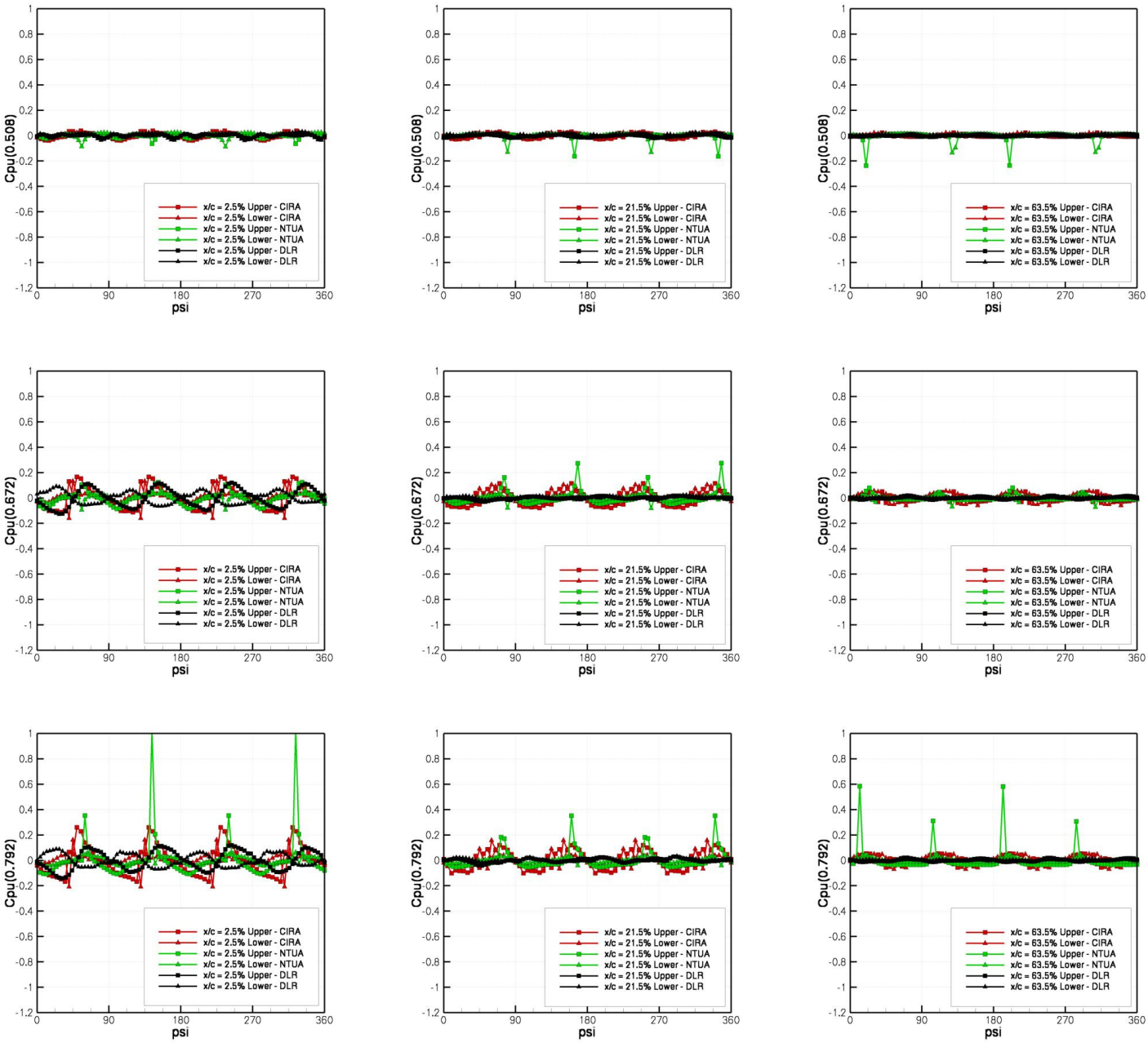

Fig 24: Comparison of the computed unsteady pressure coefficient time history on the wing for cruise flight ID7